*Progress In Electromagnetics Research, Vol. 145, 251–261, 2014*

# Investigation on Microwave Polarimetric Scattering from Two-Dimensional Wind Fetch- and Water Depth-Limited Nearshore Sea Surfaces

**Ding Nie*, Min Zhang, and Ning Li**

**Abstract**—The microwave polarimetric scattering from two-dimensional (2-D) wind fetch- and water depth-limited nearshore sea surface is investigated by using the second-order small-slope approximation (SSA-II). The sea waves are simulated by taking into account the influences of fetch and depth. Based on this, the joint influence of fetch and depth on the normalized radar cross section (NRCS) of sea surfaces for both co-polarizations and cross-polarization in different wind directions is mainly studied. Monostatic and bistatic numerical results both indicate that in the marine environment of small depth and large fetch, the nonlinear interactions among waves become more intense, which has a greater impact on NRCSs for co-polarizations than their cross-polarized counterparts. Comparison of the results for different wind directions also reflects that the backscattered echoes along wind direction have much greater strength, regardless of the magnitude of wind fetch and water depth.

## 1. INTRODUCTION

Microwave radar sea echoes can be influenced by various marine environmental factors, such as wind speed above sea surfaces, wind direction related to radar sightline, water depth, and wind fetch. With the rapid development of radar technology, the details of scattering features of radar sea echoes can be presented by radar and related means, which promotes extensive investigation on the influences of these aforementioned marine environmental factors on sea echoes. Most of the related researches focus on studying the impact of wind speed and wind directions via measurements and numerical simulations [1–9]; however, it is still far from a clear understanding of the joint influence of water depth and wind fetch on the microwave scattering. Duncan et al. [10] studied the fetch and wind speed dependence of Doppler spectra of backscattered echoes in wave tanks and found some uncontrolled factors other than fetch and wind speed would exert great influence on the Doppler spectral features. Hasselmann et al. [11] studied the observed wave growth and continuous transition from a fetch-limited to a fully developed wind-sea spectrum from the viewpoint of the experimental observations; however, the effect of water depth was not included. Bouws et al. [12] proposed a sea spectrum to describe wind waves in water of finite depth based on experimental data sets, but the corresponding microwave scattering features of echoes from these types of sea surfaces are rarely mentioned in the published studies.

Although numerical approaches such as method of moments (MoM) and related methods show much more accuracy than analytical methods, when dealing with two-dimensional (2-D) electrically large ocean surfaces, their numerical efficiency is more unsatisfactory. Some modern analytical scattering models have shown great balance between the accuracy and efficiency, such as the second-order small-slope approximation (SSA-II) model [13, 14]. Via this competent model SSA-II, the joint effect of water depth and wind fetch, which will have remarkable impact on sea waves in nearshore region, can be investigated in detail.

*Received 25 February 2014, Accepted 25 March 2014, Scheduled 1 April 2014*

* Corresponding author: Ding Nie (dnie@mail.xidian.edu.cn).
The authors are with the School of Physics and Optoelectronic Engineering, Xidian University, Xi'an 710071, China.

Both horizontal-horizontal polarization ($HH$-pol) and vertical-vertical polarization ($VV$-pol) are studied in this paper. In addition, the cross-polarization, horizontal-vertical polarization ($HV$-pol), is also investigated in the computation, which is rarely considered in recent investigations on scattering from sea surfaces. Our motivation for investigating the cross-polarized components comes from our consideration for presenting higher-order contributions rather than only the single-scattering contribution.

This paper is organized as follows. In Section 2, the geometric shapes of 2-D sea surfaces for different wind fetches and water depths, and their statistical properties are firstly simulated and analyzed. On this basis, Section 3 presents the formulation of SSA-II method for evaluating the joint influence of wind fetch and water depth on microwave sea echoes. The numerical results of the monostatic and bistatic normalized radar cross section (NRCS) of 2-D sea surfaces in different fetches and depths cases are discussed in Section 4. Section 5 concludes this paper.

## 2. FETCH- AND DEPTH-LIMITED NEARSHORE SEA SURFACE MODEL

In the field of physical oceanography, wind fetch denotes the distance that the wind has blown over open sea, and water gains energy from the wind through a long wind fetch, thus the waves grow and become a larger size. Ocean wave in nearshore region is a typical representative of the unsteady waves. Here, the 2-D sea spectrum $\Psi(f, \varphi)$ is resorted to illustrate the impacts of marine environment in the process of nearshore sea surface simulation [15],

$$\Psi(f,\varphi) = \frac{\alpha_p}{(2\pi)^4 f^5} L_p \nu_p \zeta \Phi(\varphi), \tag{1}$$

it should be stressed that all the following physical parameters in the paper are in international system of units (SI), where $f$ is the frequency of the sea wave, generalized equilibrium range parameter $\alpha_p = 0.076\tilde{X}^{-0.22}$, dimensionless fetch $\tilde{X} = gX/U_{10}^2$, $X$ the wind fetch, $U_{10}$ the the wind speed at an altitude of 10 m above the sea surface, and $g$ the gravity acceleration.

$$L_p = \exp\left[-\frac{5}{4}\left(\frac{f_p}{f}\right)^4\right], \tag{2}$$

where $f_p = 3.5g^{0.67}/(X^{0.33}U_{10}^{0.34})$ denotes the frequency of the spectral peak.

$$\nu_p = \gamma^{\rho}, \tag{3}$$

where the factors $\gamma$ and $\rho$ can be easily referred to Elfouhaily's unified sea spectrum in [16]. Based on the wave theory, it is known that the sea will be fully developed if the wind fetch is long enough, or the wind blows over sea surfaces for a large duration. Namely, if the wind fetch is smaller, the waves will be in an unsteady state. Thus the properties of waves simulated in this paper will be influenced by the wind fetch $X$ in terms of the sea spectrum in Equation (1).

According to the theory of McCormick [17], the shoaling effect on the wave height during wave propagating from deep sea to the coastal area is denoted as follows:

$$\zeta = \sqrt{\frac{\cosh^2(kd)}{\sinh(kd)\cosh(kd) + kd}}, \tag{4}$$

where $\zeta$ is the shoaling coefficient, $k$ the wavenumber of ocean waves, and $d$ the water depth. The frequency of sea wave $f$ and water depth $d$ have the relationship as follows, according to the shallow-water gravity-capillarity dispersion relation,

$$f = \sqrt{gk\left(1 + k^2/k_m^2\right)\tanh(kd)}/2\pi \tag{5}$$

with $k_m = 363.2\,\mathrm{rad/m}$.

The angle spread function in Equation (1) can be written as

$$\Phi(\varphi) = \frac{1}{2\pi}\left\{1 + \Delta_K \cos\left[2\left(\varphi - \varphi_w\right)\right]\right\}, \tag{6}$$

where $\varphi_w$ is the wind direction with respect to the radar sight line (see Figure 4).

$$\Delta_K = \tanh\left[\frac{\ln 2}{4} + 4\left(\frac{v_p}{v_{pk}}\right)^{2.5} + 0.13\frac{u_f}{v_{pm}}\left(\frac{v_{pm}}{v_p}\right)^{2.5}\right] \tag{7}$$

with $v_p = \sqrt{\frac{g}{k}[1 + (\frac{k}{k_m})^2]}$, $v_{pk} = \frac{U_{10}}{\Omega_c}$, $v_{pm} = 0.23\,\mathrm{m/s}$, $u_f$ is the friction velocity.

Figure 1 illustrates the fetch-limited sea spectrum in Equation (1) for different sea water depths. It can be clearly seen that when wind fetch increases, the spectral peak moves to the low frequency, and the energy of the spectrum also grows. It is indicated that the waves undergo a transition from a developing state to the fully developed state. In addition, when water depth decreases, the peaks of the spectra corresponding to the same wind fetch shift towards the high frequency part. These phenomena imply that under the circumstance of short wind fetch and low water depth, the shorter wind waves that have much more choppy appearances are prone to be generated.

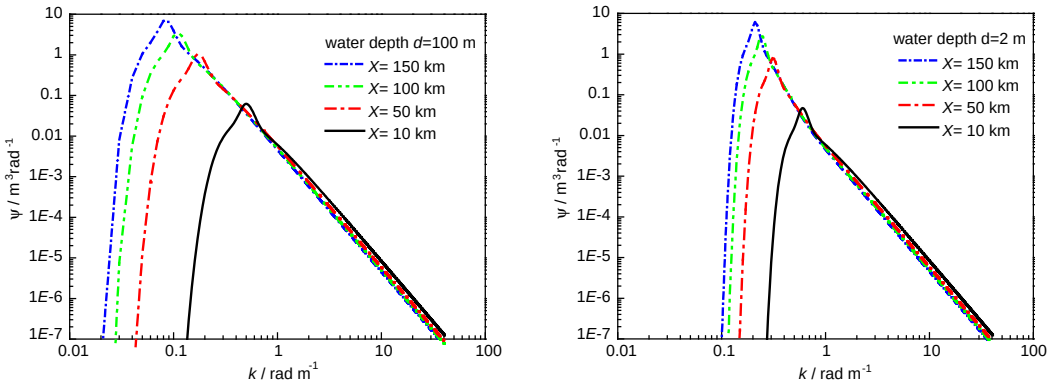


**Figure 1.** The fetch-limited sea spectra for different sea water depths. Wind speed $U_{10} = 10\,\mathrm{m/s}$: (a) $d = 100\,\mathrm{m}$, (b) $d = 2\,\mathrm{m}$.

The original choppy wave model (CWM) is revised to simulate fetch- and depth-limited nearshore sea surfaces in this paper. Based on this model, the time-varying sea surface elevation at time $t$ can be expressed as

$$h(\mathbf{r}, t) = \int \mathbf{F}(\mathbf{r}, \mathbf{k}; t)\exp(j\mathbf{k}\cdot\mathbf{r})\,\mathrm{d}\mathbf{k} \tag{8}$$

where

$$\mathbf{F}(\mathbf{r}, \mathbf{k}; t) = \frac{1}{2\pi}\left[\chi(\mathbf{k})\sqrt{\frac{\Psi(k,\varphi)}{L_x L_y}}\exp(j\omega t) + \chi(-\mathbf{k})^*\sqrt{\frac{\Psi(k,\pi-\varphi)}{L_x L_y}}\exp(-j\omega t)\right] \tag{9}$$

where vector $\mathbf{r} = (x, y)$ represents the coordinate of horizontal position, $\mathbf{k} = (k_x, k_y)$ a 2-D vector for wavenumber of ocean waves, and $|\mathbf{k}| = k$. $\Psi(k, \varphi)$ is the aforementioned sea spectrum. The corresponding definitions of other parameters can be found in [18], which we safely omit for the sake of brevity. The fetch- and depth-limited nearshore sea surfaces can be obtained by the following transformation:

$$\{\mathbf{r}, h(\mathbf{r}, t)\} \mapsto \{\mathbf{r} + \mathbf{C}_h(\mathbf{r}, t), h(\mathbf{r}, t)\}, \tag{10}$$

where the displacement $\mathbf{C}_h$ is the Riesz transform of the integral kernel $\mathbf{F}$ in Equation (9),

$$\mathbf{C}_h(\mathbf{r}, t) = \int -j\frac{\mathbf{k}}{k}\coth(kd)\,\mathbf{F}(\mathbf{r}, \mathbf{k}; t)\exp(j\mathbf{k}\cdot\mathbf{r})\mathrm{d}\mathbf{k}. \tag{11}$$

Compared with the original CWM, it should be noted that the term $\mathbf{C}_h$ in Equation (11) has been redefined to reflect the depth-limited effect via inserting the depth-related term $\coth(kd)$. Thus it is

known that the depth-limited effect plays its role via Equation (4) and Equation (11) throughout the process of waves simulations.

Figure 2 shows the simulated 2-D ocean scene of nearshore region with different wind fetches based on the fetch- and depth-limited sea spectrum in Equation (1) and the revised CWM in Equation (10). The water depth is 5 m, and wind speed is 10 m/s. It can be clearly observed from Figure 2 that the short wind fetch effect leads to a much more choppy outward appearance of ocean surface, which is attributed to the fact that the limited fetch hinders the formation of long waves and gives birth to lots of high-frequency sea shorter waves with large slopes.

To carefully explore the geometric appearance of the sea surface, the one-dimensional (1-D) profiles of simulated 2-D fetch- and depth-limited sea surface are presented in Figure 3. The wind speed is 10 m/s, and three wind fetches of 1 km, 10 km and 100 km are chosen for comparison under the circumstances of deep sea ($d = 100$ m) and nearshore sea ($d = 2$ m). Firstly, it can be clearly seen in Figure 3(a) that the sea surface elevation gradually increases as wind fetch becomes longer. A similar phenomenon can also be observed in Figure 3(b). In actual marine environment, when wind fetch grows, wind waves tend to be much more mature. Among them are high frequency waves with short wavelength and low frequency waves with much longer wavelength, and the simulations in Figure 3 just reflect this fact. Secondly, in the condition of small wind fetch (1 km), the difference between the sea surface for small water depth (2 m) and that for large water depth (100 m) is almost negligible; when fetch grows, the above difference gradually increases. At wind fetch of 100 km, the difference can be obviously observed. This indicates that the influence of water depth on the wave shape becomes much more pronounced when wind fetch increases. This is consistent with the experimental observation in [19]. Finally, to further analyze the results in Figure 3, Table 1 just gives the statistical description

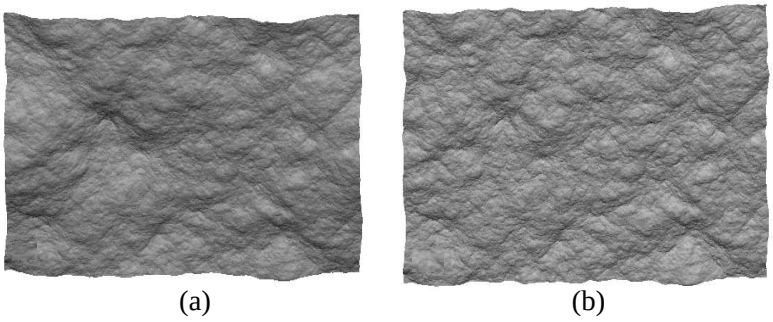


**Figure 2.** The simulated ocean scenes of nearshore region with different wind fetches. Water depth $d = 5$ m, wind speed $U_{10} = 10$ m/s: (a) $X = 100$ km, (b) $X = 5$ km.

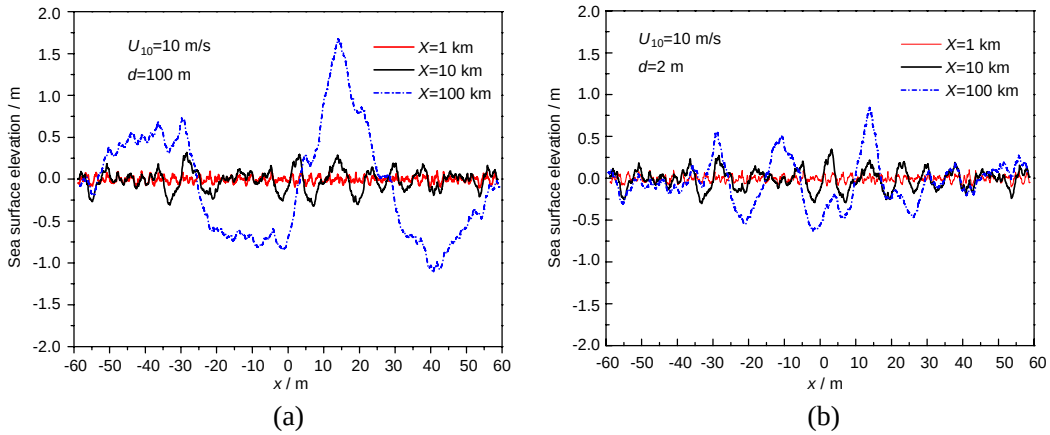


**Figure 3.** The 1-D profiles of simulated 2-D fetch- and depth-limited sea surfaces. Wind speed $U_{10}$ =10 m/s: (a) $d = 100$ m, (b) $d = 2$ m.

**Table 1.** Statistics characteristics of sea surfaces for different fetches and depths.

| | Deep sea ($d = 100\,\mathrm{m}$) | | Nearshore shallow sea ($d = 2\,\mathrm{m}$) | |
|---|---|---|---|---|
| Wind fetch (km) | RMS height (m) | RMS slope | RMS height (m) | RMS slope |
| $X = 1$ | 0.03672 | 0.23594 | 0.03661 | 0.23589 |
| $X = 10$ | 0.12480 | 0.21051 | 0.12133 | 0.21197 |
| $X = 100$ | 0.67049 | 0.19088 | 0.28801 | 0.19607 |

of the above-mentioned sea surfaces for different fetches and depths: 'RMS height' represents the root mean square of the sea surface elevation, while 'RMS slope' represents the root mean square of the sea surface slope. These data provide support for the aforementioned conclusion to some degree.

## 3. MICROWAVE SCATTERING FROM NEARSHORE SEA SURFACES

In recent years, the SSA model has been successfully utilized to evaluate the microwave scattering from rough/sea surfaces because of its good compromise between accuracy and efficiency [4, 18, 20]. Based on this consideration, the SSA-II model is exploited to theoretically analyze the microwave polarimetric scattering from fetch- and depth-limited nearshore sea surfaces.

In the far-field zone, the scattered field $\mathbf{E}_s$ above the sea surface at the distance $R$ in the general framework of the SSA theory [14] can be given by

$$\mathbf{E}_s = \mathbf{S}\mathbf{E}_i \tag{12}$$

where $\mathbf{E}_i = E_i\hat{\mathbf{E}}_0$ is the incident field, which is tapered by a Gaussian beam to avoid the edge effect caused by the finite illuminated rectangle area $L_x \times L_y$ in this paper.

$$E_i = G(x, y, h)\exp(-j\mathbf{k}_i \cdot \mathbf{r} + jq_i h) \tag{13}$$

where $G(x, y, h)$ is the taper function presented as follows

$$G(x, y, h) = \exp\left[-jk_i\left(\cos\theta_i h - x\sin\theta_i\cos\phi_i - y\sin\theta_i\sin\phi_i\right)w(x, y, h)\right]\exp(-t_x - t_y) \tag{14}$$

$$t_x = \frac{\left(\cos\theta_i\cos\phi_i x + \cos\theta_i\sin\phi_i y + \sin\theta_i h\right)^2}{g_t^2\cos^2\theta_i}, \tag{15}$$

$$t_y = \frac{\left(-\sin\phi_i x + \cos\phi_i y\right)^2}{g_t^2}, \tag{16}$$

$$w(x, y, h) = \frac{1}{k_i^2}\left[\frac{(2t_x - 1)}{g_t^2\cos^2\theta_i} + \frac{(2t_y - 1)}{g_t^2}\right], \tag{17}$$

where configuration angles ($\theta_i$, $\phi_i$, $\theta_s$, $\phi_s$) denote incident angle, incident azimuth angle, scattering angle and scattering azimuth angle respectively. $g_t$ is taper wave beam waist that controls the tapering of the incident wave. The details of other parameters can be found in [21], which we safely omit for the sake of brevity. Furthermore, $\mathbf{S}$ is the scattering matrix described as follows [14]:

$$\mathbf{S}(\mathbf{k}_s, \mathbf{k}_i) = -j\mathbf{S}_0(\mathbf{k}_s, \mathbf{k}_i)\frac{\exp(jKR)}{R}. \tag{18}$$

Referring to Figure 4, $\mathbf{K}_i = (\mathbf{k}_i, -q_i)$ is the incident wave vector, $\mathbf{K}_s = (\mathbf{k}_s, q_s)$ the scattering wave vector, and $\mathbf{k}_i$ and $\mathbf{k}_s$ are their horizontal components respectively and have relation as

$$|\mathbf{K}_i| = \sqrt{|\mathbf{k}_i|^2 + q_i^2} = \sqrt{|\mathbf{k}_s|^2 + q_s^2} = |\mathbf{K}_s| = K. \tag{19}$$

$$\mathbf{k}_i = K\left(\hat{\mathbf{x}}\sin\theta_i\cos\phi_i + \hat{\mathbf{y}}\sin\theta_i\sin\phi_i\right) \tag{20}$$

$$\mathbf{k}_s = K\left(\hat{\mathbf{x}}\sin\theta_s\cos\phi_s + \hat{\mathbf{y}}\sin\theta_s\sin\phi_s\right) \tag{21}$$

$$q_i = K\cos\theta_i \tag{22}$$

$$q_s = K\cos\theta_s \tag{23}$$

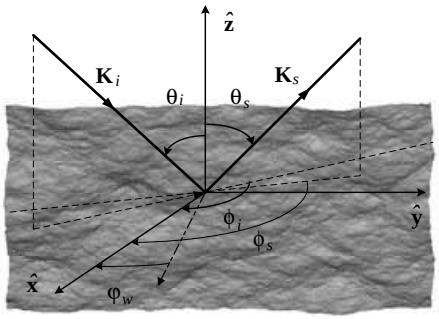


**Figure 4.** Geometry of the 2-D sea-surface scattering problem.

The scattering amplitude $\mathbf{S}_0(\mathbf{k}_s, \mathbf{k}_i)$ for the SSA-II model is then given by the following expression [18]:

$$\begin{aligned}\mathbf{S}_0(\mathbf{k}_s, \mathbf{k}_i) &= \frac{2q_i q_s}{Q\sqrt{P_i}} \int \frac{\mathrm{d}\mathbf{r}}{(2\pi)^2} G(\mathbf{r}, h) \exp\left[-j(\mathbf{k}_s - \mathbf{k}_i)\cdot(\mathbf{r} + \mathbf{C}_h(\mathbf{r}, t)) + j(q_s + q_i)h(\mathbf{r}, t)\right] \\ &\quad \times J(\mathbf{r}) \left[B_1(\mathbf{k}_s, \mathbf{k}_i) - \frac{j}{4}\int M(\mathbf{k}_s, \mathbf{k}_i; \boldsymbol{\varsigma}) H(\boldsymbol{\varsigma}) \exp(j\boldsymbol{\varsigma}\cdot\mathbf{r})\, d\boldsymbol{\varsigma}\right] \end{aligned} \tag{24}$$

where $j$ is the imaginary unit, $\frac{j}{4}\int M(\mathbf{k}_s, \mathbf{k}_i; \boldsymbol{\varsigma}) H(\boldsymbol{\varsigma}) \exp(j\boldsymbol{\varsigma}\cdot\mathbf{r}) d\boldsymbol{\varsigma}$ denotes the second-order correction to the first-order SSA theory, and $J$ is the Jacobian transformation to accomplish the change of integral variable from $\mathbf{r}$ to $(\mathbf{r} + \mathbf{C}_h(\mathbf{r}, t))$:

$$J(\mathbf{r}) = \begin{vmatrix} 1 + \frac{\partial \mathbf{C}_{hx}(\mathbf{r})}{\partial x} & \frac{\partial \mathbf{C}_{hy}(\mathbf{r})}{\partial x} \\ \frac{\partial \mathbf{C}_{hx}(\mathbf{r})}{\partial y} & 1 + \frac{\partial \mathbf{C}_{hy}(\mathbf{r})}{\partial y} \end{vmatrix}, \tag{25}$$

$$M(\mathbf{k}_s, \mathbf{k}_i; \boldsymbol{\varsigma}) = B_2(\mathbf{k}_s, \mathbf{k}_i; \mathbf{k}_s - \boldsymbol{\varsigma}) + B_2(\mathbf{k}_s, \mathbf{k}_i; \mathbf{k}_i + \boldsymbol{\varsigma}) + 2QB_1(\mathbf{k}_s, \mathbf{k}_i), \tag{26}$$

$B_1$ is the first-order Bragg kernel, and $B_2$ represents the second-order correction to the first-order solution. Their exact expressions can be found in [13]. $P_i$ is the incident wave power captured by the sea surface, $Q = q_i + q_s$, and $H(\boldsymbol{\varsigma})$ the Fourier transform of the surface elevation

$$H(\boldsymbol{\varsigma}) = \frac{1}{(2\pi)^2}\int h(\mathbf{r}) \exp(-j\boldsymbol{\varsigma}\cdot\mathbf{r}) d\mathbf{r}. \tag{27}$$

To take account of the different polarizations, the scattering amplitude is expressed as a $2 \times 2$ matrix:

$$\mathbf{S}_0(\mathbf{k}_s, \mathbf{k}_i) = \begin{bmatrix} \mathbf{S}_{0vv}(\mathbf{k}_s, \mathbf{k}_i) & \mathbf{S}_{0vh}(\mathbf{k}_s, \mathbf{k}_i) \\ \mathbf{S}_{0hv}(\mathbf{k}_s, \mathbf{k}_i) & \mathbf{S}_{0hh}(\mathbf{k}_s, \mathbf{k}_i) \end{bmatrix}. \tag{28}$$

Since the microwave scattering from sea surfaces is a stochastic problem, then the NRCS is defined as follows:

$$\sigma = \lim_{R\to\infty} 4\pi R^2 \left\langle |\mathbf{S}(\mathbf{k}_s, \mathbf{k}_i)|^2 \right\rangle, \tag{29}$$

the brackets $\langle\cdot\rangle$ denotes the ensemble average over much surface realizations.

## 4. NUMERICAL RESULTS AND DISCUSSION

Comparison of the NRCS of the ordinary deep sea surfaces calculated by SSA-II with the exact numerical simulation has been already presented in the published references [4, 22], thus the SSA-II model is safely used to evaluate the NRCS of fetch- and depth-limited nearshore sea surfaces in the following simulations.

The microwave scattering features of nearshore 2-D sea surfaces will be analyzed based on SSA-II model. The monostatic NRCSs of fetch- and depth-limited 2-D sea surfaces are depicted in Figure 5.

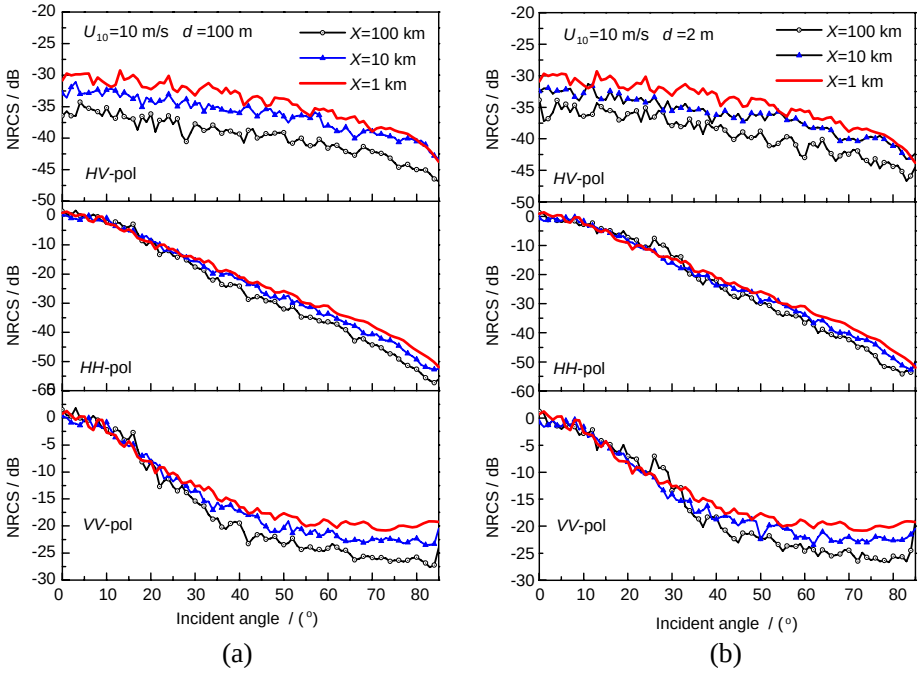


**Figure 5.** Monostatic NRCSs versus incident angle for fetch- and depth-limited 2-D sea surfaces in upwind direction. The incident frequency is 1.304 GHz: (a) $d = 100\,\text{m}$, (b) $d = 2\,\text{m}$.

The final NRCSs are averaged over 80 surface realizations, where the incident frequency is 1.304 GHz, the permittivity of sea water (72.1, 71.0), the wind speed 10 m/s in upwind direction, the size of the simulated surface $L_x \times L_y$ $256\lambda \times 256\lambda$ ($\lambda$ is wavelength), the sampling interval $\lambda/8$, and the taper wave beam waist $g_t$ is chosen to be $L_x/6$. The water depths are set to 100 m for deep sea and 2 m for shallow sea in nearshore region, and for comparison, the wind fetches are set as 1 km, 10 km, and 100 km, respectively. Both of the co-polarizations ($HH$-pol, $VV$-pol) and cross-polarization ($HV$-pol) are investigated in detail.

In the case of deep sea ($d = 100\,\text{m}$), it can be observed that the NRCSs for co-polarizations ($HH$-pol, $VV$-pol) have nearly the same value in small angle region (0° to 20°); then, the curves obviously decrease as the wind fetch increases for both co-polarizations at the remaining incident angle region. However, in the case of nearshore sea ($d = 2\,\text{m}$), the most notable differences take place in the angle region of 20° to 30° for both co-polarizations: NRCSs for fetch $X = 100\,\text{km}$ are greater than those for fetch $X = 1\,\text{km}$. In the nearshore shallow water, the effect of finite depth becomes significant for larger fetch, and the nonlinear interactions among waves are more intense, i.e., the wave crests will become much steeper than their counterparts in the deep sea, which is consistent with the measurement observations in [19, 23] and also can be reflected from Table 1. Thus, the backscattered echoes will be much stronger than those in the deep sea under the same large fetch condition (e.g., $X = 100\,\text{km}$). Meanwhile, the small fetch suppresses the growths of waves in both deep sea and nearshore shallow sea environment, which leads to almost negligible difference in these two cases. The joint effect of above two aspects leads to the aforementioned phenomenon, which is also supported by the analysis in [24]. When incident angle exceeds 30°, the variation trend of curves is similar to the counterpart of deep sea. After all, the diffuse-backscattering will be dominated by small-scale short waves with large slopes, thus it is obvious that the NRCSs increase under the decreasing fetches circumstance at the moderate and large incident angles (30° to 80°), whether for deep sea or for nearshore shallow sea.

As for the case for cross-polarization ($HV$-pol), the curves present a similar variation trend throughout the whole angles for both deep sea and shallow sea situations: NRCSs decrease with increasing wind fetches, which may imply that the mechanism of Bragg scattering rather than the nonlinear interaction dominates the variation of NRCSs with incident angle for the cross-polarization case.

The influence of the joint effect of water depth and wind fetch on NRCSs of sea surfaces for different wind directions are shown in Figure 6. Two typical wind directions are chosen for comparison: upwind direction (UW) and crosswind direction (CW), and the water depth and wind fetch are set as $d = 2\,\mathrm{m}$, $d = 100\,\mathrm{m}$, $X = 1\,\mathrm{km}$, $X = 100\,\mathrm{km}$, respectively. The incident frequency is 1.304 GHz. It is obvious that the curves for upwind direction are much higher than those for crosswind direction at most incident angles, regardless of the magnitude of $d$ and $X$. This phenomenon can be explained by the fact that the wave crests always tilt toward the direction of the wind, thus the roughnesses and slopes of the sea surfaces for the upwind direction case will be greater than those for the crosswind direction case. In addition, an even more interesting phenomenon is that the differences of NRCSs for co-polarizations between different wind directions are significant for large fetch situation ($X = 100\,\mathrm{km}$) in the angle region of 10° to 30°, especially for small depth $d = 2\,\mathrm{m}$ condition. This phenomenon also reflects that the nonlinear interactions between short waves will be greatly strengthened in shallow sea under large wind fetches circumstance. For the cross-polarization case, the variation trends of the curves are similar for the upwind and crosswind direction cases in four plots, which reflects from the other side that the aforementioned nonlinear effect has a slight impact on the NRCSs for cross-polarization, while the Bragg scattering influences the NRCSs for cross-polarization most.

To comprehensively investigate the joint effect of water depth and wind fetch, the bistatic scattering configuration is also analyzed. Figure 7 displays the variation of NRCSs with scattering angle for forward-backward bistatic scattering configuration. The parameters of marine environment and scattering environment are similar to those in Figure 5, except that the incident angle is 70° here. For the co-polarizations cases, when $d = 100\,\mathrm{m}$, it can be clearly seen that the NRCSs decrease with increasing wind fetches while scattering angle departing from the specular direction, which is caused by the fact that the slopes of waves become much more gentle for larger fetches, which will reduce the

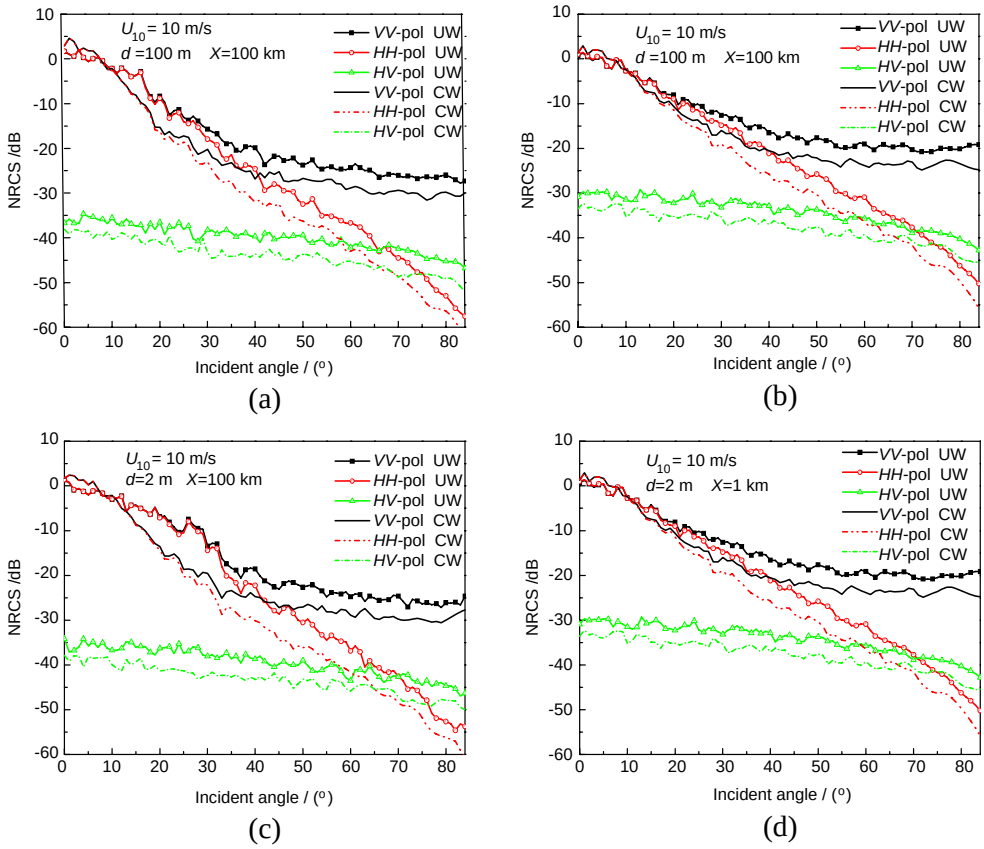


**Figure 6.** The influence of the joint effect of water depth and wind fetch on monostatic NRCSs of sea surfaces for different wind directions: upwind (UW) and crosswind (CW).

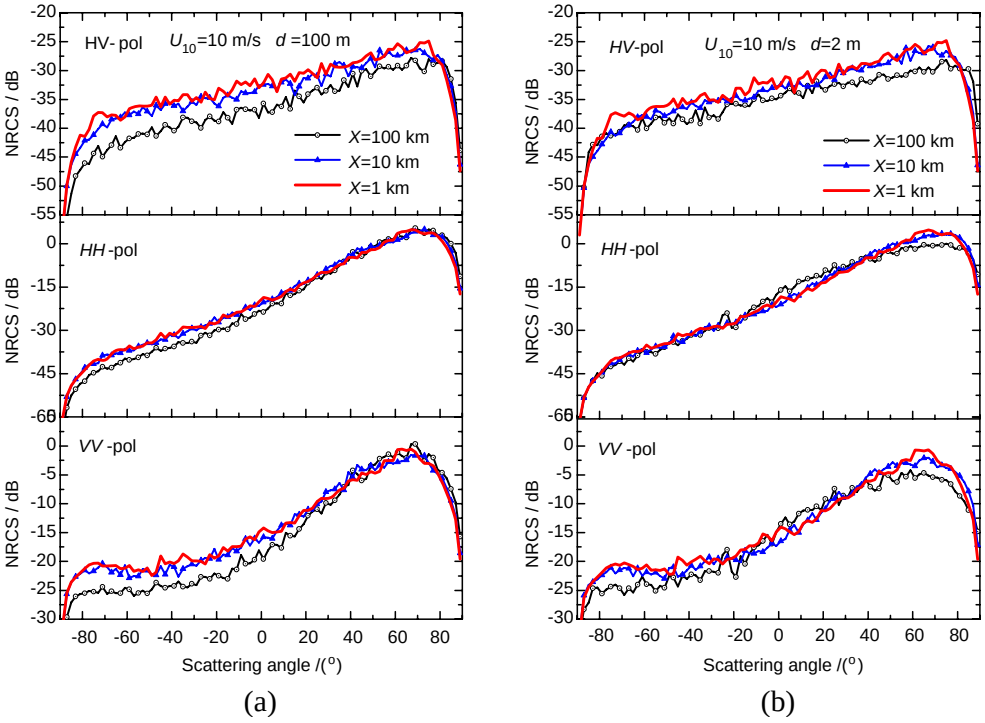


**Figure 7.** Bistatic NRCSs versus scattering angle for fetch- and depth-limited 2-D sea surfaces in upwind direction. The incident frequency is 1.304 GHz: (a) $d = 100\,\mathrm{m}$, (b) $d = 2\,\mathrm{m}$.

intensity of backscattered echoes. As for the case of $d = 2\,\mathrm{m}$, in the angle region of $-10^\circ$ to $30^\circ$, the curves for large fetches are higher than those for small fetch, and this phenomenon is caused by the strengthened nonlinear interactions between waves, which is similar to the situation in the backscattering configuration. For the cross-polarization case, NRCSs decrease with increasing wind fetches, which is also consistent with the variation trend of the curves in the backscattering configuration in Figure 5.

## 5. CONCLUSION

This paper presents an investigation of microwave polarimetric scattering features of echoes from 2-D fetch- and depth-limited nearshore sea surfaces. The sea spectrum that takes the influences of limited wind fetch and shoaling effect into account is utilized to construct more realistic coastal sea surface by the revised nonlinear CWM model. Then the joint impact of wind fetch and water depth to the NRCSs of dynamic sea surfaces for both co-polarizations and cross-polarization is studied.

Based on the simulation and discussion, it is found that in deep sea or nearshore shallow sea, the variation of NRCSs with incident angle for the same wind fetch shows different trends. It is indicated that in the marine environment of small water depth and large wind fetch, the nonlinear interactions among sea waves become much more intense, which has a greater impact on NRCSs for co-polarizations than those for cross-polarization. Based on the comparison of simulation results for upwind direction case with those for crosswind direction case, it is clearly shown that the backscattered echoes along wind direction have much greater strength, regardless of the magnitude of wind fetch and water depth. Finally, the bistatic scattering from fetch- and depth-limited nearshore sea surfaces is investigated in detail.

This paper deals with not only the water depth-limited effect, but also the wind fetch-limit effect in the scattering from 2-D nearshore sea surfaces. Moreover, the cross-polarization scattering is also investigated, which will help to better investigate the microwave scattering from complex nearshore seas. Future work should be carried out to study the characteristics of Doppler spectra from 2-D fetch- and depth-limited sea surfaces.

## ACKNOWLEDGMENT

The authors would like to thank the Fundamental Research Funds for the Central Universities and the National Natural Science Foundation of China under Grant Nos. 41306188 and 61372004 to support this kind of research.

## REFERENCES

1. Kitaigorodskii, S. A., V. P. Krasitskii, and M. M. Zaslavskii, "On Phillips' theory of equilibrium range in the spectra of wind-generated gravity waves," *J. Phys. Oceanogr.*, Vol. 5, No. 3, 410–420, 1975.
2. Schroeder, L. C., P. R. Schaffner, J. L. Mitchell, and W. L. Jones, "AAFE RADSCAT 13.9-GHz measurements and analysis: Wind-speed signature of the ocean," *IEEE J. Ocean. Eng.*, Vol. 10, No. 4, 346–357, 1985.
3. Wentz, F. J., S. Peteherich, and L. A. Thomas, "A model function for ocean radar cross-section at 14.6 GHz," *J. Geophys. Res.*, Vol. 89, 3689–3704, 1984.
4. Zhang, Y. M., Y. H. Wang, and L. X. Guo, "Study of scattering from time-varying Gerstners sea surface using second-order small slope approximation," *Chin. Phys. B*, Vol. 19, No. 5, 054103, 2010.
5. Bringer, A., B. Chapron, A. Mouche, and C. A. Guérin, "Revisiting the short-wave spectrum of the sea surface in the light of the weighted curvature approximation," *IEEE Trans. Geosci. Remote Sens.*, Vol. 52, No. 1, 679–689, 2014.
6. Luo, H. J., G. D. Yang, Y. H. Wang, J. C. Shi, and Y. Du, "Numerical studies of sea surface scattering with the GMRES-RP method," *IEEE Trans. Geosci. Remote Sens.*, Vol. 52, No. 4, 2064–2073, 2014.
7. Isoguchi, O. and M. Shimada, "A L-band ocean geophysical model function derived from PALSAR," *IEEE Trans. Geosci. Remote Sens.*, Vol. 47, No. 7, 1925–1936, 2009.
8. McDaniel, S. T., "Microwave backscatter from non-Gaussian seas," *IEEE Trans. Geosci. Remote Sens.*, Vol. 41, No. 1, 811–817, 2003.
9. Young, I. R., S. Zieger, and A. V. Babmin, "Global trends in wind speed and wave height," *Science*, Vol. 332, No. 6028, 451–455, 2011.
10. Duncan, J. W., W. C. Keller, and J. W. Wright, "Fetch and windspeed dependence of Doppler spectra," *Radio Sci.*, Vol. 9, 809–819, 1974.
11. Hasselmann, S., K. Hasselmann, J. H. Allender, and T. P. Barnett, "Computations and parameterizations of the nonlinear energy transfer in a gravity-wave specturm. Part II: Parameterizations of the nonlinear energy transfer for application in wave models," *J. Phys. Oceanogr.*, Vol. 15, 1378–1391, 1978.
12. Bouws, E., H. Günther, W. Rosenthal, and C. L. Vincent, "Similarity of the wind wave spectrum in finite depth water: 1. Spectral form," *J. Geophys. Res.*, Vol. 90, 975–986, 1985.
13. Voronovich, A. G. and V. U. Zavorotny, "Theoretical model for scattering of radar signals in Ku- and C-bands from a rough sea surface with breaking waves," *Waves Random Media*, Vol. 11, 247–269, 2001.
14. Elfouhaily, T. M. and C. A. Guérin, "A critical survey of approximate scattering wave theories from random rough surfaces," *Waves Random Media*, Vol. 14, R1–R40, 2004.
15. Hasselmann, K., et al., "Measurements of wind-wave growth and swell decay during the Joint North Sea Wave Project (JONSWAP)," *Dtsch. Hydrogr. Z. Suppl.*, Vol. 12, No. A8, 1–95, 1973.
16. Elfouhaily, T. M., B. Chapron, K. Katsaros, and D. Vandemark, "A unified directional spectrum for long and short wind-driven waves," *J. Geophys. Res.*, Vol. 102, 15781–15796, 1997.
17. McCormick, M. E., *Ocean Engineering Wave Mechanics*, John Wiley & Sons Inc., New York, 1973.
18. Nie, D., M. Zhang, C. Wang, and H. C. Yin, "Study of microwave backscattering from two-dimensional nonlinear surfaces of finite-depth seas," *IEEE Trans. Geosci. Remote Sens.*, Vol. 50, No. 11, 4349–4357, 2012.

19. Young, I. R. and L. A. Verhagen, "The growth of fetch limited waves in water of finite depth. Part 1. Total energy and peak frequency," *Coast. Eng.*, Vol. 29, 47–78, 1996.
20. Bourlier, C., "Azimuthal harmonic coefficients of the microwave backscattering from a non-Gaussian ocean surface with the first-order SSA model," *IEEE Trans. Geosci. Remote Sens.*, Vol. 42, No. 11, 2600–2611, 2004.
21. Tsang, L., J. A. Kong, and K. H. Ding, *Scattering of Electromagnetic Waves,* John Wiley & Sons Inc., New York, 2001.
22. Toporkov, J. V. and G. S. Brown, "Numerical study of the extended Kirchhoff approach and the lowest order small slope approximation for scattering from ocean-like surfaces: Doppler analysis," *IEEE Trans. Antennas Propag.*, Vol. 50, No. 4, 417–425, 2002.
23. Ross, D. and W. L. Jones, "On the relationship of radar backscatter to wind speed and fetch," *Bound Layer Meteorol.*, Vol. 13, 151–163, 1978.
24. Ward, K. D. and R. Tough, "Modelling radar sea clutter in littoral environments," *2008 IEEE International Conference on Radar*, 82–87, 2008.